Manawwer Alam*, Eram Sharmin, Naser M. Alandis and Naushad Ahmad

# Effect of organoclay on structure, morphology, thermal behavior and coating performance of Jatropha oil based polyesteramide

DOI 10.1515/epoly-2017-0096
Received May 15, 2017; accepted June 19, 2017; previously published online July 29, 2017

**Abstract:** Jatropha oil (JO) is an inedible oil mainly used in biodiesel. We have attempted to prepare a JO-based polyesteramide/clay composite using a one-pot, two-step reaction, for application as a protective coating. The aim of the work is to utilize JO for its value-added application by preparing a JO polyesteramide/clay composite, to investigate the potential of the prepared composite as a protective coating, and also to study the effect of loaded clay on the structure, morphology, thermal stability and coating properties of the composite. The formation of composites was confirmed by Fourier transform infrared spectroscopy (FTIR), transmission electron microscopy (TEM) and atomic force microscope (AFM) studies. The coating properties were studied by standard physico-mechanical and corrosion resistance tests in corrosive media (3.5 wt% HCl, 3.5 wt% NaCl and tap water). The thermal stability was assessed by differential scanning calorimetry (DSC), thermogravimetric (TGA) and derivative thermogravimetric (DTG) analyses. The coatings showed good physico-mechanical and corrosion resistance performance and can be safely used up to 275°C. The approach paves way towards an alternate value addition to a non-edible oil.

**Keywords:** coatings; composite; clay; Jatropha oil; polyesteramide.

## 1 Introduction

Biocomposites comprise a biobased organic polymer matrix and inorganic nanofillers. They show improved thermal and mechanical properties, corrosion resistance, fire retardance and biodegradability, with wide applications especially in the field of packaging materials, structural materials, medical devices, antimicrobial, corrosion resistant coatings, paints and others (1–7). Several biopolymers such as chitosan (8), starch (9), cellulose (10), polylactic acid (11), vegetable oils (VO) and their derivatives (12, 13) have been widely used as polymer matrices with nanosized fillers such as silica, clay, carbon nanotubes and others.

Montmorillonite (MMT) is the most commonly used clay; it is a crystalline 2:1 layered clay mineral with a central alumina octahedral sheet sandwiched between two silica tetrahedral sheets, with high aspect ratio. MMT is either intercalated or exfoliated by polymer chains to form biocomposites (14–16). Such material is generally used as an additive to improve some physical properties of polymers and to provide reinforcement to polymer matrices. The type and content of MMT influences the final properties of biocomposites (17–19).

VO polymer/clay composites are one of the most promising biocomposite materials. These have been prepared by epoxidation (20–24), acrylation (14, 25, 26), styrenation, vinylation (27–30), esterification (31–33) and urethanation (34, 35) of VO, followed by their nanocomposite formation with organoclay in different doses. Such intercalated or exfoliated organoclay VO bionanocomposites have shown improved mechanical properties (14), thermal stability (14, 21, 32, 34), water barrier properties (34–37), biodegradability (32, 34), non-cytotoxicity (34), antimicrobial activity (33), flame retardancy (38), transparency and light weight characteristics (35) compared to the pristine VO polymers, which generally lack rigidity, strength and thermostability (25, 32, 39). The reinforcing effect of the organoclay modifier depends on the polarity, flexibility, structure and feed ratio (21, 26) of monomers as well as strong interfacial interactions between the biopolymer matrix and layered silicates (40, 41). Heidarian et al. (42) have prepared castor oil polyurethane/MMT nanocomposites through ultrasonication assisted process, and studied the corrosion protection performance of their coatings by electrochemical measurements. Zafar and coworkers synthesized polyurethanamide nanocomposite by *in situ* polymerization of linseed oil derived diol fattyamide and tolulylene-2,4-diisocyanate in the presence of different

***Corresponding author: Manawwer Alam,** Research Centre-College of Science, King Saud University, P.O. Box 2455, Riyadh 11451, Saudi Arabia, e-mail: malamiitd@gmail.com
**Eram Sharmin:** Department of Pharmaceutical Chemistry, College of Pharmacy, Umm Al-Qura University, P.O. Box 715, Makkah Al-Mukarramah 21955, Saudi Arabia
**Naser M. Alandis and Naushad Ahmad:** Department of Chemistry, College of Science, King Saud University, P.O. Box 2455, Riyadh 11451, Saudi Arabia

contents of organic montmorillonite (OMMT) at room temperature (43), with good coating properties such as scratch hardness (3.5 kg), impact resistance (passes 200 lb/inch) and bend test values (passes 1/8 inch).

Polyesteramides are amide modified alkyds. They have been obtained from VO such as linseed, castor, soy, *Pongamia glabra*, corn, olive and others. VO based polyesteramides contain ester, amide and pendant alkyl chains (from parent oil). These functional groups impart good adhesion, flexibility, thermal stability and chemical resistance (specially against acid media), and also provide functional group sites for chemical modification, thus rendering the polymer useful in protective coatings (42, 44–47). These have been modified by the introduction of acrylic moieties, boron, aluminum, urethane, and others for improved physico-mechanical performance and chemical resistance (47, 48). Zafar et al. (49) recently developed linseed oil based waterborne polyesteramide/MMT bionanocomposites via a microwave (MW)-assisted technique. However, as linseed oil is also used for edible purposes, the approach would be more fruitful and its value would be augmented many times, if it is applied to oils that are non-edible, such as Jatropha oil (JO). In the present study, we have developed JO based polyesteramide/MMT clay nanocomposites. The approach focuses on the utilization of a non-edible oil for alternate value-added commercial application in paints and coatings. It is a motivating step towards sustainability and value-addition.

# 2 Experimental

## 2.1 Chemicals and instrumentations

JO (50), MMT (particle size 2–13 μm, layer thickness 1 nm), Cloisite 30B; Southern Clay Products, Gonzales, USA), Phthalic anhydride (Hopkins, Plainville, England), diethanolamine (Fluka Chemie, Switzerland), sodium metal, methanol (Sigma Aldrich, Louis, USA), were used as received.

The physico-chemical analyses of nanocomposites such as the determination of acid value (ASTM D555-61), and refractive index (ASTM D1218) were carried out by standard ASTM laboratory methods. Fourier transform infrared (FTIR) measurements were conducted on a FTIR spectrometer, Spectrum 100 (Perkin Elmer Cetus Instrument, Norwalk, CT, USA) using an NaCl cell with a wave number resolution of 2 $cm^{-1}$ at room temperature. Morphological studies were carried out by transmission electron microscopy (TEM) (JEM-2100F). Topography was measured by atomic force microscope (AFM) in the noncontact mode (TriA SPM, A.P.E. Research, Trieste, Italy). Thermogravimetric analysis (TGA) and differential scanning calorimetry (DSC) were carried out by TGA/DSC1 (Mettler Toledo AG, Analytical CH-8603, Schwerzenbach, Switzerland) in nitrogen atmosphere to investigate the thermal degradation pattern of the polymers. Physico-mechanical properties of coated panels such as the scratch hardness (BS 3900), adhesion test by cross hatch (ASTM D3359-02), the impact test (IS 101 part 5 $s^{-1}$, 1988), the flexibility/bending test (ASTM D3281-84), the pencil hardness test (ASTM D3363-05), the salt spray test (ASTM B117) and the thickness (ASTM D 1186-B) were measured. The corrosion resistance of JPEA coatings was measured by the use of a conventional three electrode cell system, calomel was used as a reference electrode, platinum as a counter electrode and coated and bare mild steel (MS) panel as a working electrode (exposed area 1 $cm^2$). Tafel data were collected by using a Gill AC (ACM Instruments, UK) and the potential range ±250 mV with a scanning rate 5 mV/s (51).

## 2.2 Synthesis of N,N-bis(2-hydroxy ethyl) Jatropha oil fatty amide (HEJA)

Synthesis of HEJA was performed according to previously reported papers (50, 52). JO was treated with diethanolamine in the presence of sodium methoxide, at 150°C. The reaction was monitored by thin layer chromatography (TLC), at regular intervals of time. After the reaction was complete, the product was washed with diethyl ether and sodium choride solution. HEJA was obtained by base catalyzed amidation of JO. HEJA is an amide, functionalized with two hydroxyl groups and a pendant alkyl chain of oil.

## 2.3 Synthesis of Jatropha oil polyesteramide (JPEA)/MMT clay composites and their coatings

The formation of JPEA and its composite occurred by a one-pot, two-step reaction. MMT clay was soaked for 24 h in deionized water before the reaction. HEJA (0.028 mol), MMT (1–4 wt% on the weight of HEJA) and methanol were placed in a three-necked flask and vigorously stirred for 90 h at 50°C. This was done for proper mixing of the MMT clay with a monomer. After this time period, phthalic anhydride (0.028 mol) was added in the same reaction flask in small pinches, and the reaction temperature was raised to 180°C; the reaction was continued at this temperature for

5 h. The reaction was monitored by recording acid values and by FTIR taken at regular intervals. A series of polyesteramide resins, JPEA-1, JPEA-2, JPEA-3 and JPEA-4 was prepared, where the last digit indicated the percent loading of MMT. A similar reaction was performed without the addition of MMT, to prepare plain JPEA. In this reaction, JPEA preparation and the clay intercalation/exfoliation in the polymer occurred in a one-pot (in same reaction vessel). HEJA hydroxyls reacted with carboxylic groups of phthalic anhydride forming JPEA, followed by intercalation/exfoliation of MMT clay in the polymer. JPEA, JPEA-1, JPEA-2, JPEA-3 and JPEA-4 were applied on MS strips and were baked/stoved at 200°C for 1 h, to prepare their coatings.

# 3 Results and discussion

HEJA was treated with phthalic anhydride and MMT clay, in different percentages (1–3 wt%) producing polyesteramide composites. In the first step, HEJA reacted with phthalic anhydride forming JPEA as shown in Scheme 1, followed by the interaction of synthesized JPEA with MMT clay platelets. Beyond 3 wt%, the coating properties deteriorated, thus only composites up to 1–3 wt% clay inclusions are studied here. Acid values (8–12, 18) decreased from JPEA to JPEA-3, the trend showed descending order from JPEA > JPEA-1 > JPEA-2 > JPEA-3. Refractive index values (1.5024, 1.5300, 1.5310–1.5312) increased from JPEA to JPEA-3, the trend showed ascending order from JPEA < JPEA-1 < JPEA-2 < JPEA-3. These values show noticeable increase, on increasing the amount of MMT clay.

## 3.1 FTIR

The FTIR spectrum of JO (Figure 1) shows the characteristic absorption bands at 3009 $cm^{-1}$ (-C=C-CH, str.), 2918, 2853 $cm^{-1}$ (-$CH_3$, $CH_2$ sym and asym str.), 1750 $cm^{-1}$ (>C=O, str of ester carbonyl), 1235, 1161 $cm^{-1}$ (-C-O str of triester). In HEJA (Figure 1), along with the absorption bands observed in JO at 3007 $cm^{-1}$ (-C=C-CH-, str), 2924, 2853 $cm^{-1}$ (-$CH_3$, $CH_2$ sym and asym, str.), additional absorption bands are observed at 3349 $cm^{-1}$ (-OH), 1621 $cm^{-1}$ (amide carbonyl) along with the suppression of bands at 1750 (>C=O, str of ester carbonyl), 1235,1161 [-C-C-(=O)-O-C str. of ester], that supports the amidation reaction at ester groups of JO, and the formation of amide diol.

In the spectrum of JPEA (Figure 1), characteristic absorption bands at 3425 $cm^{-1}$ (broad OH), 1730 $cm^{-1}$ (>C=O ester), 1637 $cm^{-1}$ (>C=O, amide), 1273, 1138 $cm^{-1}$ (-C-O ester str), 1070 $cm^{-1}$ (C-O primary alcohol), 1600–1580 $cm^{-1}$ and 746 $cm^{-1}$ (Ar-C=C-H) appear along with the bands occurring in the spectrum of JO. These peaks support the esterification reaction of HEJA with phthalic anhydride forming polyesteramide resin. MMT clay (Figure 2) shows peaks at 3694–3620 $cm^{-1}$ (OH stretching of Al-OH), 1630 $cm^{-1}$ (hydrogen bonded water bending), 1018 $cm^{-1}$ (broad Si-O stretching), 542 $cm^{-1}$ (Si-O-Al bending), 468 $cm^{-1}$ (Si-O-Si stretching) (40). The spectrum of JPEA-3 shows the peaks at 3383 $cm^{-1}$ (broad, OH), 1725 $cm^{-1}$ (>C O, ester), 1614 $cm^{-1}$ (>C O, amide carbonyl), 1275 $cm^{-1}$ (-C-O- ester), 1071–1050 $cm^{-1}$ (Si-O str. and C-O- primary alcohol), 1105 (Si-O-Si, asym str.), 528 $cm^{-1}$ (Si-O-Al) and 449 $cm^{-1}$ (Si-O-Si sym str.). The shifting of bands is observed in the case of hydroxyls, esters and amide carbonyls, respectively, in JPEA-3 as compared

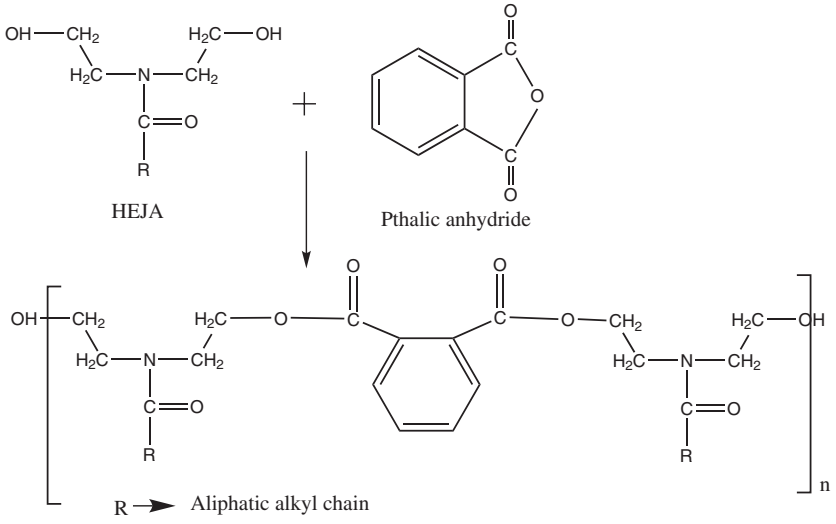


**Scheme 1:** Synthesis of JPEA.

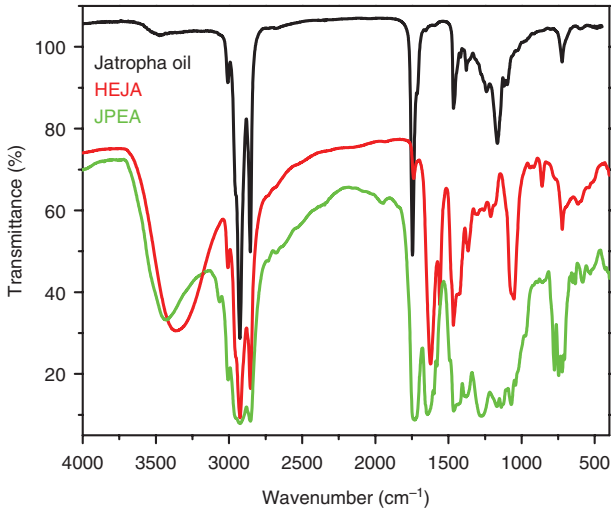


**Figure 1:** FTIR spectra of Jatropha oil, HEJA and JPEA.

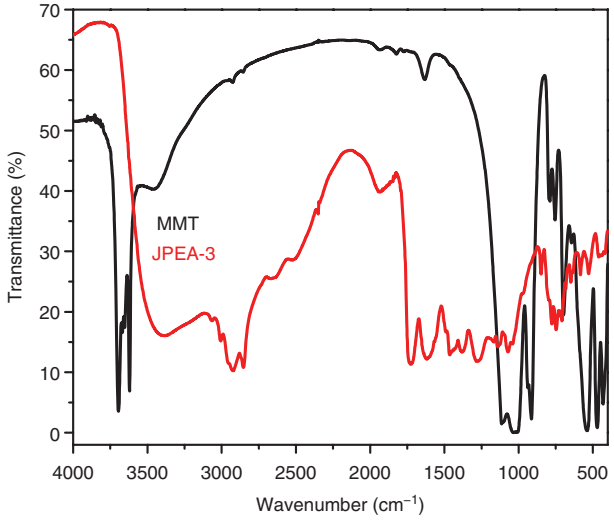


**Figure 2:** FTIR spectra of pure MMT and JPEA-3.

to JPEA, due to hydrogen bonding between these functional groups in JPEA-3 backbone and OMMT.

## 3.2 TEM analysis

The TEM micrograph (Figure 3) of JPEA-3 reveals that (dark) nanometer sized clay platelets are surrounded by a (gray) sheath of JPEA chains, which shows that there are greater interactions occurring between JPEA chains and MMT clay platelets (as also supported by FTIR results) arising due to the intercalation of clay platelets by JPEA chains (1.50). There are polar groups (free hydroxyls and carboxyls) present in JPEA backbone that allow for hydrogen bonding with clay platelets. In X-ray diffraction (XRD)

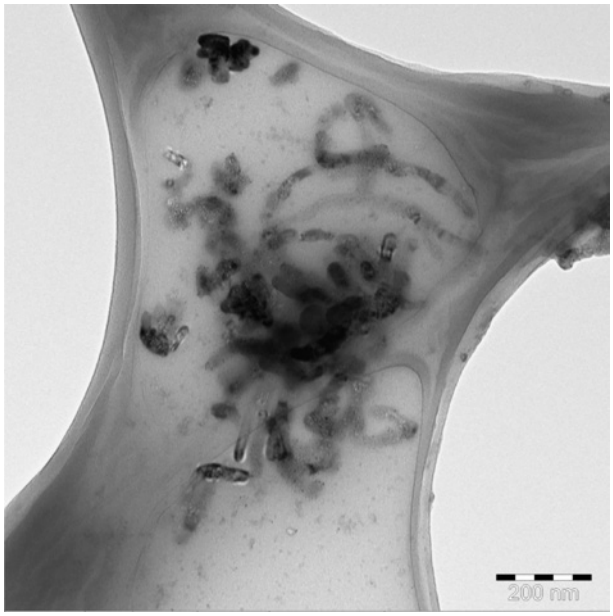


**Figure 3:** TEM micrograph of JPEA-3.

(not shown here), no typical characteristic peak of OMMT clay is observed in the 2θ range from 5 to 40° (53), showing that the clay platelets are well intercalated by polyesteramide chains (54).

## 3.3 Topography

Figure 4A–C show the topography of JPEA, JPEA-3 and JPEA-3 after exposure to salt spray test/3.5 wt% NaCl, respectively. The topography of JPEA shows a smooth surface with nanoscale roughness (15 nm) and surface uniformity, while JPEA-3 also shows smooth surface and nanoscale roughness (20 nm) and surface uniformity of the coating after the addition of 3% OMMT in JPEA. JPEA-3 image very clearly indicates that clay particles are evenly dispersed in the polymer matrix. There seems to be a good connection between clay particles and the polymer resin. This also indicates improvement in the properties of corrosion resistance. The AFM topography image (Figure 4C) after exposure in 3.5 wt% NaCl solution indicates the coating surface with nanoscale roughness (35 nm) and shows some defects in coatings like pinholes, pores and increased surface roughness.

## 3.4 Thermal analysis

TGA thermograms of JPEA and JPEA-3 are shown in Figure 5. The initial 5 wt% loss observed at 279°C to 316°C

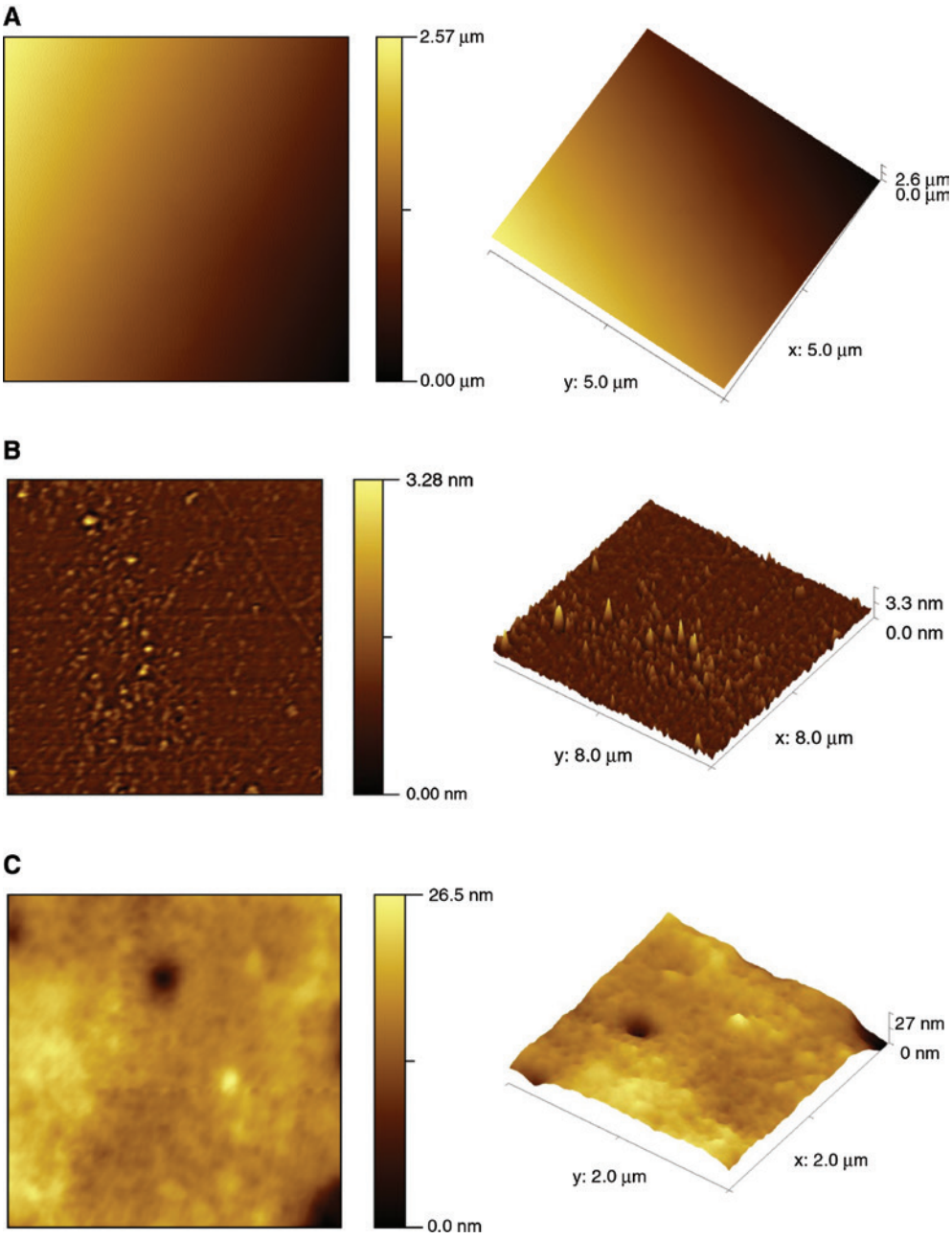


**Figure 4:** (A) AFM topographic image of JPEA coating, (B) AFM topographic image of JPEA-3 coating, (C) AFM topographic image after exposed JPEA-3 coating surface in the salt spray chamber.

can be correlated to the evaporation of the trapped moisture. A 10 wt% loss was observed at 318°C and 345°C in JPEA, and JPEA-3, 50 wt% loss due to thermal degradation was observed at 425°C in JPEA and at 441°C in JPEA-3, respectively. DTG thermograms (Figure 6) of JPEA and JPEA-3 show one endothermic peak starting from 250°C to 550°C and centered at 432°C. This endothermic peak is centered in the temperature range corresponding to 50% weight loss in the TGA thermogram. In JPEA-3, degradation temperatures are higher compared to those observed in JPEA. In JPEA and JPEA-3, the corresponding residues (10.57%, 7.311%) are also observed in their respective thermograms. The composite coatings show higher thermal stability than plain JPEA. This is a consequence of good interfacial interactions between JPEA and MMT clay platelets in composite coating, barrier property and heat insulation offered by MMT platelets. These composite coatings may be safely employed up to 275°C.

DSC thermograms of JPEA and JPEA-3 (Figure 7) show the first endothermic event at approximately 75°C,

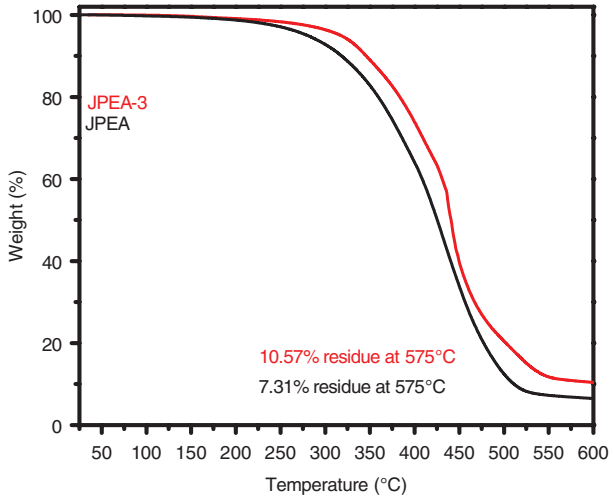


**Figure 5:** TGA thermogram of JPEA and JPEA-3.

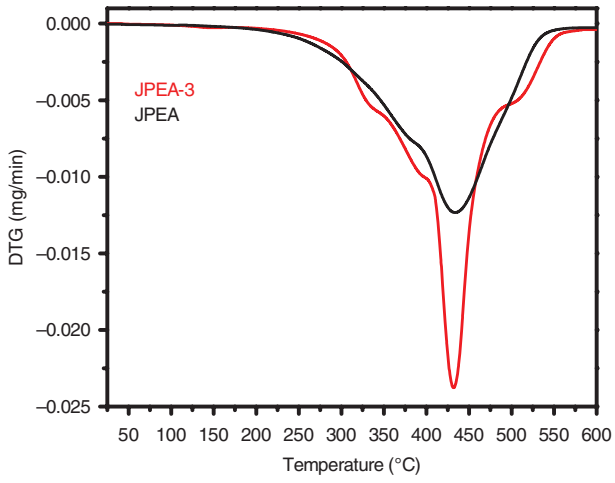


**Figure 6:** DTG thermogram of JPEA and JPEA-3.

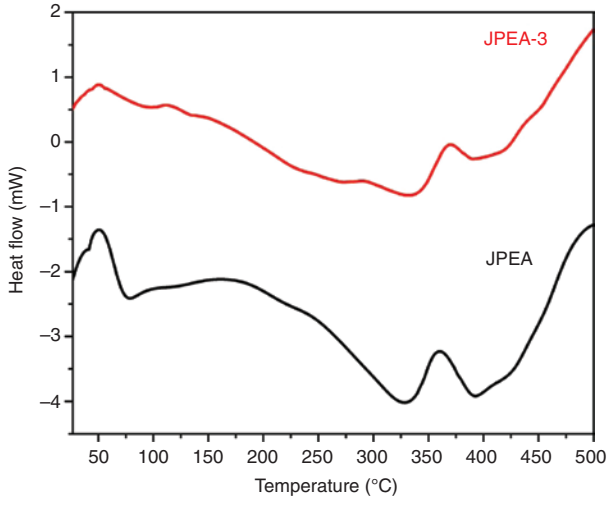


**Figure 7:** DSC thermogram of JPEA and JPEA-3.

correlated to melting of the resin, followed by another two broad endotherms between 246°C–360°C and 370°C–450°C, followed by an exotherm. These events may occur due to the configurational changes in polymers under the effect of temperature, such as the melting of polymer chains, chain scission or thermal degradation.

## 3.5 Physico-mechanical properties

The coatings were prepared by baking/stoving at 200°C for 1 h. The thickness of the coatings was found to be 155–180 µm. The scratch hardness values of coatings increased from JPEA (1.5 kg), JPEA-1 (2.0 kg), JPEA-2 (2.5 kg) and JPEA-3 (3.0 kg), beyond which the scratch hardness value deteriorated. The pencil hardness values were found to be 2B (JPEA), 3H (JPEA-1), 5H (JPEA-2), 5H (JPEA-3) and deteriorated beyond JPEA-3. The deterioration in performance beyond 3 wt% loading of MMT is a consequence of agglomeration of clay platelets at higher loading. The coatings showed good impact resistance (150 lb/inch), bending ability (1/8 inch) and cross hatch test showed 100%. The thickness of JPEA, JPEA-1, JPEA-2 and JPEA-3 coating ranged between 116 and 150 ± 5 µm.

## 3.6 Corrosion studies

Tafel polarization studies (Figure 8) of bare MS, JPEA-1,JPEA-2, and JPEA-3 coated MS were conducted after immersion for 240 h in 3.5 wt% NaCl solution. Corrosion parameters about the corrosion potential (*Ecorr*), corrosion rate (CR), polarization resistance (Rp), corrosion current density (*Icorr*) were measured by the Tafel extrapolation method. The Tafel polarization curves demonstrate that

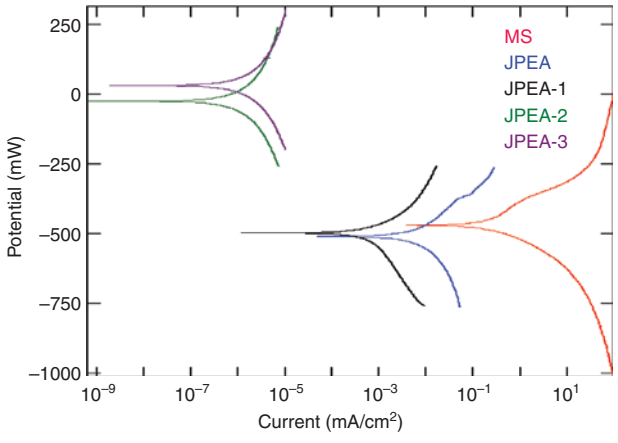


**Figure 8:** Tafel graph of bare MS and JPEA coated MS in 3.5% HCL.

**Table 1:** Tafel analysis parameters of JPEA composite coated and bare mild steel in different corrosive media.

| Code | Medium | *Ecorr* (mV) | *Icorr* (mA/cm²) | Ba (mV) | Bc (mV) | CR (mm/year) | Rp (Ohm.cm²) |
|---|---|---|---|---|---|---|---|
| MS | 3.5%NaCl | −770.84 | 0.063 | 37.390 | 27.124 | 0.738 | 107.230 |
| JPEA | 3.5%NaCl | −712.49 | 1.629E−03 | 26.167 | 31.082 | 1.888E−02 | 3790.900 |
| JPEA-1 | 3.5%NaCl | −613.84 | 1.082E−07 | 39.320 | 40.535 | 1.254E−06 | 8.019E+7 |
| JPEA-2 | 3.5%NaCl | −565.10 | 1.179E−07 | 38.413 | 44.009 | 1.213E−06 | 7.567E+7 |
| JPEA-3 | 3.5%NaCl | −160.14 | 3.478E−06 | 54.467 | 72.944 | 4.031E−06 | 3.898E+6 |
| MS | 3.5%HCl | −468.50 | 2.207 | 81.606 | 57.049 | 25.588 | 6.612 |
| JPEA | 3.5%HCl | −510.42 | 8.026E−03 | 78.158 | 75.514 | 9.302E−02 | 2080.500 |
| JPEA-1 | 3.5%HCl | −481.93 | 8.737E−03 | 57.710 | 51.127 | 10.125E−02 | 1349.100 |
| JPEA-2 | 3.5%HCl | −27.23 | 2.817E−07 | 46.487 | 43.943 | 3.265E−06 | 3.487E+7 |
| JPEA-3 | 3.5%HCl | 30.25 | 4.954E−07 | 52.167 | 60.364 | 5.741E−06 | 2.456E+7 |
| MS | Tap water | −571.09 | 3.441E−03 | 39.168 | 53.567 | 3.988−02 | 28.584E+5 |
| JPEA | Tap water | −162.67 | 3.797E−07 | 59.806 | 65.522 | 4.401E−06 | 3.581E+7 |
| JPEA-1 | Tap water | −137.56 | 3.717E−07 | 41.593 | 38.525 | 4.308E−06 | 2.340E+7 |
| JPEA-2 | Tap water | −112.45 | 2.425E−06 | 48.693 | 48.981 | 2.810E−05 | 43.788E+5 |
| JPEA-3 | Tap water | −5.16 | 6.637E−08 | 60.380 | 61.757 | 7.693E−07 | 2.000E+8 |

the JPEA-1, JPEA-2 and JPEA-3 composite coatings cause a positive displacement in *Ecorr*, relative to the value of the bare MS and JPEA coating. Table 1 indicates the corrosion parameters for bare MS and coated MS. It is clear *Ecorr*, Rp increases from bare MS to JPEA, JPEA-1, JPEA-2 and JPEA-3 and *Icorr* decreases. These results indicate JPEA coating can act as a protective barrier of MS and improve the corrosion performance, on increasing the amount of clay. This shift in the corrosion potential confirms the good protection of the MS by the barrier action of coatings. Tafel measurements clearly show a substantial reduction in CR for JPEA-3 coated MS (4.031E-06 mpy) with respect to bare MS (0.738 mpy).

Figure 9, shows the potentiodynamic polarization curve after immersion for 195 h in 3.5 wt% HCl corrosive media. *Ecorr* values of JPEA, JPEA-1, JPEA-2 and JPEA-3 coated MS are −468, −510.42, −481.93, −27.232 mV and 30.252 mV, respectively. These values shifted to more positive values, while increasing the amount of OMMT in JPEA than bare MS. In contrast, Table 1 indicates that *Icorr* values of JPEA, JPEA-1, JPEA-2 and JPEA-3 coated MS decreased gradually and Rp values increased. The *Ecorr*, *Icorr*, Rp values trends shown here indicate the corrosion resistant nature of the composite coating. The MS coated with composite coatings show remarkable improvement in corrosion resistance properties of bare MS surface. It is therefore due to the presence of clay platelets in the JPEA matrix that act as a protective agent and reduce the interaction between Cl ions and MS surface (53).

The Tafel polarization curve (Figure 10), indicates corrosion protection of JPEA, JPEA-1, JPEA-2 and JPEA-3 nanocomposite coatings on MS. The determination of *Ecorr*, Rp and *Icorr* values was performed after immersion of coated samples in tap water ($Cl^-$ ion 164 ppm) for 30 h. As listed in Table 1, JPEA, JPEA-1, JPEA-2, JPEA-3 coated MS

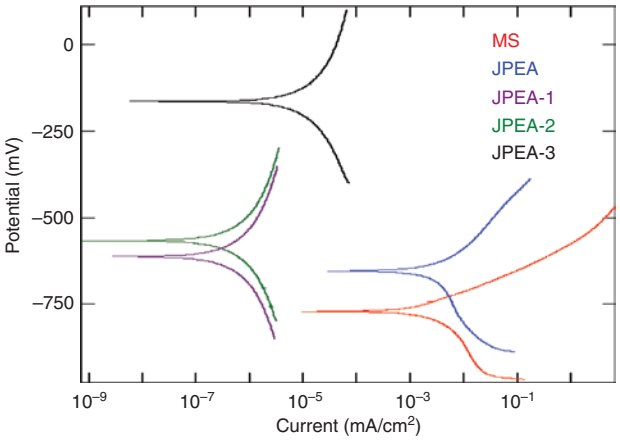


**Figure 9:** Tafel graph of bare MS and JPEA coated MS in 3.5% NaCl.

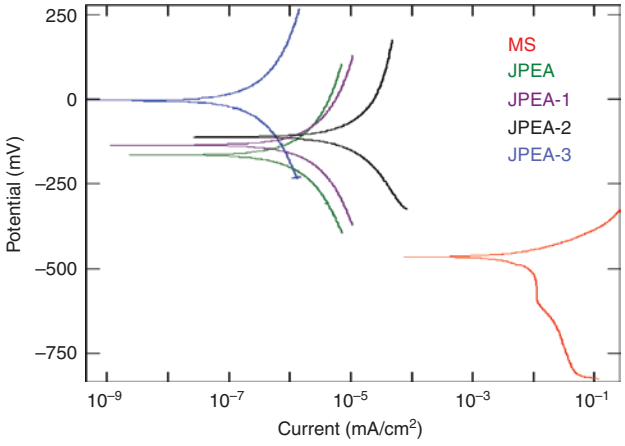


**Figure 10:** Tafel graph of bare MS and JPEA coated MS in tap water.

samples exhibits higher *Ecorr* (–571.09, –162.67, –137.56, –112.45, –5.1627 mV) value than the bare MS (–571.09 mV). The *Ecorr* values of nanocomposite coated panels increase with increasing the amounts of clay and also show higher values of Rp and smaller values of *Icorr* than JPEA coated MS strips. Again, these effects are enhanced as the clay loading is increased up to 3 wt%, revealing that anticorrosive property of the JPEA film has been enhanced due to the dispersion of clay in JPEA. The corrosion protection effect is attributed to an increase in tortuosity of the diffusion pathways of water and oxygen molecules due to the presence of the dispersed silicate particles (40).

Corrosion resistance processes of polymeric coating are barrier protection for corrosive ions. The composite coatings provide protection to the metal substrate in the following ways: (i) the presence of the pendant alkyl chain of JO, polar functionalities in JPEA coatings bring strong interactions between the coating and MS substrates leading to the formation of well-adhered and compact coating on the metal surface, (ii) the clay platelets present in JPEA act as a barrier for the corrosive ion to the metal interface and act as a filler providing a locking effect at the interstitial spaces. Hence, the protection mechanism for composite coatings was governed by adhesion, barrier and locking effects of nanofillers, which inhibits the corrosion ions permeability, and enhances the corrosion-protection efficiency of coatings (55, 56).

## 4 Conclusions

Jatropha polyesteramide was reinforced with clay platelets that improved the physico-mechanical and corrosion resistance performance of the polyesteramide composite coatings. The thermal stability of the composite coatings was better than the plain Jatropha polyesteramide coatings. The coatings performed well when tested under acid, salt and tap water as corrosive media. The mechanism of corrosion protection followed barrier action, wherein the coatings provided barrier to the permeability of corrosive media. These coatings can be safely employed up to 275°C.

**Acknowledgment:** The Project was supported by King Saud University, Deanship of Scientific Research, College of Science – Research Center.

## References

1. Bordes P, Pollet E, Avérous L. Nano-biocomposites: biodegradable polyester/nanoclay systems. Prog Polym Sci. 2009;34:125–55.
2. Sinha Ray S, Bousmina M. Biodegradable polymers and their layered silicate nanocomposites: in greening the 21st century materials world. Prog Mater Sci. 2005;50:962–79.
3. Liu D, Shi Z, Matsunaga M, Yin J. DSC investigation of the hindered effect on curing behavior for epoxy-phenol/MMT nanocomposites based on the acidic octadecylamine modifier. Polymer 2006;47:2918–27.
4. Langat J, Bellayer S, Hudrlik P, Maupinc PH, Gilman Sr JW, Raghavan D. Synthesis of imidazolium salts and their application in epoxy montmorillonite nanocomposites. Polymer 2006;47:6698–6709.
5. Haq M, Burgueño R, Mohanty AK, Misra M. Bio-based polymer nanocomposites from UPE/EML blends and nanoclay: development, experimental characterization and limits to synergistic performance. Compos Part A Appl Sci Manuf. 2011;42:41–9.
6. Da Silva EE, Della Colleta HHM, Ferlauto AS, Moreira RL, Resende RR, Oliveira S, Kitten GT, Lacerda RG, Ladeira LO. Nanostructured 3-D collagen/nanotube biocomposites for future bone regeneration scaffolds. Nano Research. 2009;2:462–73.
7. Kumar A, Vemula PK, Ajayan PM, John G. Silver-nanoparticle-embedded antimicrobial paints based on vegetable oil. Nat Mater. 2008;7:236–41.
8. Al-Sagheer F, Muslim S. Thermal and mechanical properties of chitosan/SiO2 hybrid composites. J Nanomaterials. 2010;2010:1–7.
9. Avella M, De Vlieger JJ, Errico ME, Fischer S, Vacca P, Volpe MG. Biodegradable starch/clay nanocomposite films for food packaging applications. Food Chem. 2005;93:467–74.
10. Li M, Kim IH, Jeong YG. Cellulose acetate/multiwalled carbon nanotube nanocomposites with improved mechanical, thermal, and electrical properties. J App Polym Sci. 2010;118:2475–81.
11. Wen X, Zhang K, Wang Y, Han L, Han C, Zhang H, Chen S, Dong L. Study of the thermal stabilization mechanism of biodegradable poly(L-lactide)/silica nanocomposites. Polym Int. 2011;60:202–10.
12. Deka H, Karak N, Kalita RD, Buragohain AK. Biocompatible hyperbranched polyurethane/multi-walled carbon nanotube composites as shape memory materials. Carbon 2010;48:2013–22.
13. Sravendra R, Niranjan K, Jae Whan C, Young Ho K. Enhanced dispersion of carbon nanotubes in hyperbranched polyurethane and properties of nanocomposites. Nanotechnology 2008;19:495707.
14. Lu Y, Larock RC. Novel Biobased Nanocomposites from Soybean Oil and Functionalized Organoclay. Biomacromolecules. 2006;7:2692–2700.
15. Kim YH, Kim DS. Effects of organic modifications of clay on the ultraviolet-curing behavior and structure of a polyester-acrylate/clay nanocomposite system. Polym Adv Technol. 2008;19:1236–41.
16. Jalilian M, Yeganeh H, Haghighi MN. Preparation and characterization of polyurethane electrical insulating coatings derived from novel soybean oil-based polyol. Polym Adv Technol. 2010;21:118–27.
17. Kornmann X, Lindberg H, Berglund LA. Synthesis of epoxy–clay nanocomposites: influence of the nature of the clay on structure. Polymer 2001;42:1303–10.
18. Kumar P, Sandeep KP, Alavi S, Truong VD, Gorga RE. Effect of type and content of modified montmorillonite on the structure

and properties of bio-nanocomposite films based on soy protein isolate and montmorillonite. J Food Sci. 2010;75:N46–56.
19. Park K-W, Kim G-H, Chowdhury SR. Improvement of compression set property of ethylene vinyl acetate copolymer/ethylene-1-butene copolymer/organoclay nanocomposite foams. Polym Eng Sci. 2008;48:1183–90.
20. Miyagawa H, Misra M, Drzal LT, Mohanty AK. Novel biobased nanocomposites from functionalized vegetable oil and organically-modified layered silicate clay. Polymer 2005;46:445–53.
21. Tsujimoto T, Uyama H, Kobayashi S. Synthesis of high-performance green nanocomposites from renewable natural oils. Polym Degrad Stab. 2010;95:1399–1405.
22. Uyama H, Kuwabara M, Tsujimoto T, Nakano M, Usuki A, Kobayashi S. Green nanocomposites from renewable resources: plant oil-clay hybrid materials. Chem Mater. 2003;15:2492–94.
23. Liu Z, Erhan SZ, Xu J. Preparation, characterization and mechanical properties of epoxidized soybean oil/clay nanocomposites. Polymer 2005;46:10119–27.
24. Uyama H, Kuwabara M, Tsujimoto T, Nakano M, Usuki A, Kobayashi S. Organic-inorganic hybrids from renewable plant oils and clay. Macromol Biosci. 2004;4:354–60.
25. Şen S, Çaylı G. Synthesis of bio-based polymeric nanocomposites from acrylated epoxidized soybean oil and montmorillonite clay in the presence of a bio-based intercalant. Polym Int. 2010;59:1122–9.
26. Lu J, Hong CK, Wool RP. Bio-based nanocomposites from functionalized plant oils and layered silicate. J Polym Sci Part B Polym Phy. 2004;42:1441–50.
27. Lu Y, Larock RC. Bio-based nanocomposites from corn oil and functionalized organoclay prepared by cationic polymerization. Macromol Mater Eng. 2007;292:863–72.
28. Kundu PP, Larock RC. Montmorillonite-filled nanocomposites of tung oil/styrene/divinylbenzene polymers prepared by thermal polymerization. J Appl Polym Sci. 2011;119:1297–1306.
29. Sharma V, Banait JS, Larock RC, Kundu PP. Synthesis and characterization of linseed oil-based nanocomposites. Polym Compo. 2010;31:630–7.
30. Bhuyan S, Sundararajan S, Lu Y, Larock RC. A study of the physical and tribological properties of biobased polymer–clay nanocomposites at different clay concentrations. Wear 2010;268:797–802.
31. Konwar U, Karak N. Mesua ferrea L. Seed oil based highly branched environment friendly polyester resin/clay nanocomposites. J Polym Env. 2011;19:90–9.
32. Konwar U, Karak N, Mandal M. Mesua ferrea L. seed oil based highly thermostable and biodegradable polyester/clay nanocomposites. Polym Degrad Stab. 2009;94:2221–30.
33. Konwar U, Karak N, Mandal M. Vegetable oil based highly branched polyester/clay silver nanocomposites as antimicrobial surface coating materials. Prog Org Coat. 2010;68:265–73.
34. Dutta S, Karak N, Saikia JP, Konwar BK. Biocompatible epoxy modified bio-based polyurethane nanocomposites: mechanical property, cytotoxicity and biodegradation. Bioresour Technol. 2009;100:6391–7.
35. Deka H, Karak N. Vegetable oil-based hyperbranched thermosetting polyurethane/clay nanocomposites. Nanoscale Res Lett. 2009;4:758–65.
36. Krook M, Albertsson AC, Gedde UW, Hedenqvist MS. Barrier and mechanical properties of montmorillonite/polyesteramide nanocomposite. Polym Eng Sci. 2002;42:1238–46.
37. Ahmadi Z. Interfacial interaction exploration and oxygen barrier potential of polyethylene/poly(ethylene-co-vinyl alcohol)/clay hybrid nanocomposites. e-Polymers 2017;17:175–86.
38. Das G, Karak N. Vegetable oil-based flame retardant epoxy/clay nanocomposites. Polym Degrad Stab. 2009;94:1948–54.
39. Liu X, Zhang J. High-performance biobased epoxy derived from rosin. Polym Int. 2010;59:607–9.
40. Cheng A, Wu S, Jiang D, Wu F, Shen J. Study of elastomeric polyurethane nanocomposites prepared from grafted organic-montmorillonite. Colloid Polym Sci. 2006;284:1057–61.
41. Tien YI, Wei KH. Hydrogen bonding and mechanical properties in segmented montmorillonite/polyurethane nanocomposites of different hard segment ratios. Polymer 2001;42:3213–21.
42. Heidarian M, Shishesaz MR, Kassiriha SM, Nematollahi M. Characterization of structure and corrosion resistivity of polyurethane/organoclay nanocomposite coatings prepared through an ultrasonication assisted process. Prog Org Coat. 2010;68:180–8.
43. Zafar F, Zafar H, Sharmin E. Vegetable oil based polyurethanamide/organo-montmorillonite bio-nanocomposite. J Appl Polym Sci. 2014;131. Doi: 10.1002/app.4028.
44. Petrović ZS. Polyurethanes from vegetable oils. Polym Rev. 2008;48:109–55.
45. Akram D, Sharmin E, Ahmad S. Synthesis, characterization and corrosion protective properties of boron-modified polyurethane from natural polyol. Prog Org Coat. 2008;63:25–32.
46. Akram D, Sharmin E, Ahmad S. Development and characterization of boron incorporated linseed oil polyurethanes. J Appl Polym Sci. 2010;116:499–508.
47. Akram D, Ahmad S, Sharmin E, Ahmad S. Silica reinforced organic–inorganic hybrid polyurethane nanocomposites from sustainable resource. Macromol Chem Phys. 2010;211:412–9.
48. Narges T, Soheil S. Effect of clay loading on the structural and mechanical properties of organoclay/HDI-based thermoplastic polyurethane nanocomposites. e-Polymers 2016;16:65–74.
49. Zafar F, Sharmin E, Zafar H, Shah MY, Nishat N, Ahmad S. Facile microwave-assisted preparation of waterborne polyesteramide/OMMT clay bio-nanocomposites for protective coatings. Ind Crops Prod. 2015;67:484–91.
50. Alam M, Alandis NM. Microwave assisted synthesis of urethane modified polyesteramide coatings from jatropha seed oil. J Polym Env. 2011;19:784–92.
51. Alam M, Alandis NM, Ahmad N, Naushad M. Synthesis and characterization of poly(urethane-ether azomethine) fatty amide based corrosion resistant coatings from pongamia glabra oil: an eco-friendly approach. J Chem. 2016;2016:1–10.
52. Alam M, Alandis NM. Microwave-assisted preparation of urethane-modified polyetheramide coatings from Jatropha seed oil. High Perform Polym. 2012;24:538–45.
53. Sari MG, Ramezanzadeh B, Shahbazi M, Pakdel AS. Influence of nanoclay particles modification by polyesteramide hyperbranched polymer on the corrosion protective performance of the epoxy nanocomposite. Corros Sci. 2015;92:162–72.

54. Ratna D, Becker O, Krishnamurthy R, Simon GP, Varley RJ. Nanocomposites based on a combination of epoxy resin, hyperbranched epoxy and a layered silicate. Polymer 2003;44:7449–57.
55. Solarski S, Benali S, Rochery M, Devaux E, Alexandre M, Monteverde F, Dubois, P. Synthesis of a polyurethane/clay nanocomposite used as coating: interactions between the counterions of clay and the isocyanate and incidence on the nanocomposite structure. J Appl Polym Sci. 2005;95:238–44.
56. Pirvu C, Demetrescu I, Drob P, Vasilescu E, Vasilescu C, Mindroiu M, Stancuc R. Electrochemical stability and surface analysis of a new alkyd paint with low content of volatile organic compounds. Prog Org Coat. 2010;68: 274–82.